ELSEVIER

Biochimica et Biophysica Acta 1566 (2002) 28–43

BIOCHIMICA ET BIOPHYSICA ACTA
BBA

www.bba-direct.com

Review

Mitochondria-rich cells as experimental model in studies of epithelial chloride channels

Niels J. Willumsen[a], Jan Amstrup[a], Nadja Møbjerg[b], Åse Jespersen[b], Poul Kristensen[c], E. Hviid Larsen[a,*]

[a] *Zoophysiological Laboratory, August Krogh Institute, University of Copenhagen, Universitetsparken 13, DK-2100 Copenhagen Ø, Denmark*
[b] *Department of Zoomorphology, Zoological Institute, University of Copenhagen, Universitetsparken 5, DK-2100 Copenhagen Ø, Denmark*
[c] *Biochemical Department, August Krogh Institute, University of Copenhagen, Universitetsparken 13, DK-2100 Copenhagen Ø, Denmark*

Received 6 June 2002; accepted 19 July 2002

Abstract

The mitochondria-rich (mr) cell of amphibian skin epithelium is differentiated as a highly specialised pathway for passive transepithelial transport of chloride. The apical membrane of mr cells expresses several types of Cl^- channels, of which the function of only two types has been studied in detail. (i) One type of channel is gated by voltage and external chloride concentration. This intriguing type of regulation leads to opening of channels only if $[Cl^-]_o$ is in the millimolar range and if the electrical potential is of a polarity that secures an inwardly directed net flux of this ion. Reversible voltage activations of the conductance proceed with long time constants, which depend on V in such a way that the rate of conductance activation increases when V is clamped at more negative values (serosal bath grounded). The gating seems to involve processes that are dependent on F-actin localised in the submembrane domain in the neck region of the flask-shaped mr cell. (ii) The other identified Cl^- pathway of mr cells is mediated by small-conductance apical CFTR chloride channels as concluded from its activation via β-adrenergic receptors, ion selectivity, genistein stimulation and inhibition by glibenclamide. *bb*CFTR has been cloned, and immunostaining has shown that the gene product is selectively expressed in mr cells. There is cross-talk between the two pathways in the sense that activation of the conductance of the mr cell by voltage clamping excludes activation via receptor occupation, and vice versa. The mechanism of this cross-talk is unknown.

Keywords: *Bufo bufo*; Mitochondria-rich cell; Voltage-activated Cl^- channel; β-Adrenergic receptor; Cyclic AMP; CFTR; Patch clamp; Noise analysis; Cytochalasin D; Actin

1. Introduction

Principal cells of high-resistance epithelia like the amphibian skin [1] and the distal renal epithelia [2] are specialised for active uptake of Na^+ energized by a basolateral Na/K-ATPase. Generally, apical Na^+ uptake via amiloride blockable epithelial Na^+ channels (ENaC) dominates the function of these epithelia [3–5], but also a potassium secretory pathway has been disclosed in the amphibian skin [6] and in the collecting duct system [2]. Furthermore, during a body load of K^+, the apical exit pathway is activated [6–11] and in the terrestrial European toad, *Bufo bufo*, potassium secretion is a major function of both collecting tubules and collecting ducts [12]. In amphibian skin [13] and rat collecting duct [14], the apical plasma membrane of principal cells does not exhibit a chloride conductance, and the intracellular chloride activity of this cell type is above electrochemical equilibrium. Obviously therefore, principal cells do not constitute the route for transepithelial uptake by electrodiffusion of Cl^- that follows the active uptake of Na^+. As another common feature, these epithelia are not only heterofunctional as indicated above, but also heterocellular with minority cell types interspersed among the principal cells. The minority cell type is denoted intercalated cells in the kidney [15–17], and mitochondria-rich (mr) cells in amphibian skin [18], urinary bladder [19], and fish gill [20]. In distal renal epithelia, intercalated cells have been associated with the elimination of acid (A-, or α-cells) and base (B-, or β-cells), energized by a H-ATPase [21], and with active uptake of K^+ driven by an H/K-ATPase

* Corresponding author. Tel.: +45-3532-1642; fax: +45-3532-1567.
E-mail address: ehlarsen@aki.ku.dk (E.H. Larsen).

0005-2736/02/$ - see front matter
PII: S0005-2736(02)00591-6

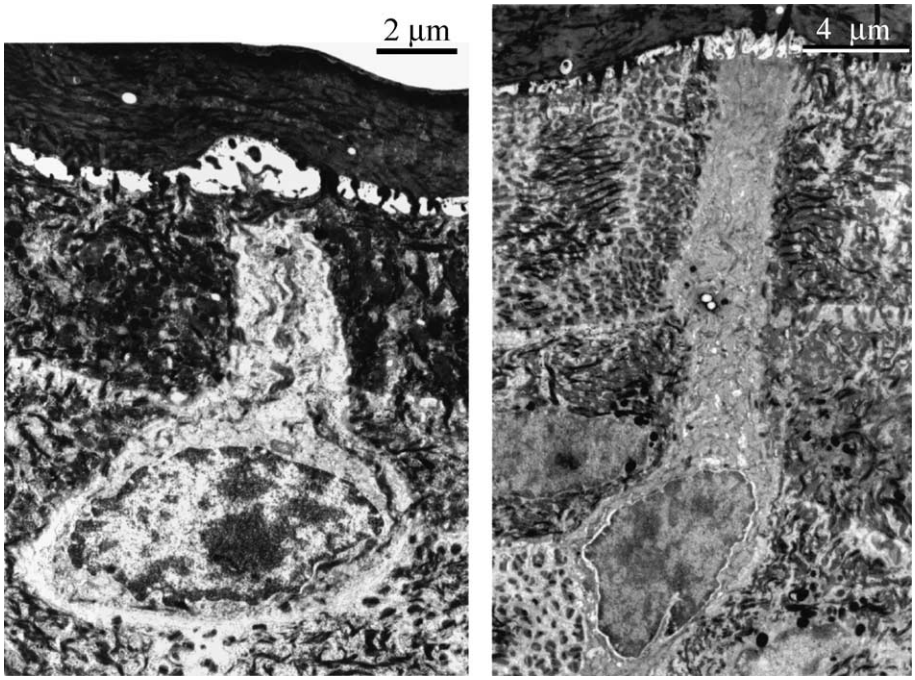

Fig. 1. Transmission electron microscopic pictures of mr cells from the toad (*B. bufo*) epidermis. The neck of the mr cell is situated between the outermost layer of sodium-transporting cells so that its apical membrane is at the same level as the sodium selective membrane (with ENaC) of principal cells. Both cell types are covered by a dead *stratum corneum*, which is freely permeable to electrolytes and small diffusible molecules. The mr cell is usually flask shaped (left-hand panel), but also long, slender cells are seen (right-hand panel). The cell body of mr cells containing the cell nucleus is located in the layers below the outermost living cell layer. For methods, see Ref. [53].

[22]. In the amphibian skin, a type of mr cells is differentiated for selective uptake of Cl^- (Fig. 1), but depending on the physiology of the organism, it is likely that functions similar to those of kidney intercalated cells are expressed in subpopulations of mr cells (reviewed in Ref. [23]). When toads are forced into negative chloride balance, the pool of mr cells of the skin increases, and the density reaches a new steady state within a few days after onset of the challenge [24,25]. The chloride conductance of the fully differentiated mr cell becomes activated when the electrochemical gradient favours a passive net influx of Cl^- [26], and it is inactivated when the animal is in freshwater of low Cl^- concentration [27] where the uptake of Cl^- is active.[1] This regulation proceeds with a much shorter time constant (seconds, minutes). Another equally fast regulation of the chloride conductance of mr cells is initiated by occupation of β-adrenergic receptors [30]. The mr cell of the skin epithelium, therefore, provides an excellent experimental model for the study of cellular and molecular regulation of chloride channels of a heterocellular epithelium. In this review, we discuss Cl^- channels and their regulatory mechanisms that have been associated with this cell type.

[1] Proton-ATPase-driven ion transports in mr cells are discussed in Refs. [28,29], and in Section 6 of this review.

2. The voltage-dependent Cl^- conductance of mr cells

2.1. Macroscopic features

The polarized nature of the *V*-dependent mechanism is revealed by clamping the transepithelial electrical potential difference, *V*, to −80 or +80 mV from a holding potential of 0 mV (see Fig. 2A). The sodium ions of the external bath were here substituted by potassium ions so that the major current component is carried by Cl^- (I_{Cl}). Stepping *V* from 0 to −80 mV, that is, into the physiological range of transepithelial potentials, slowly activated I_{Cl}, from −30 to −80 μA/cm^2. In contrast, following a step change of *V* to +80 mV, the current deactivated. Fig. 2B shows a series of current activations obtained by stepping *V* from a holding potential of 50 mV to values ranging from 25 to −100 mV. The amplitude of the activated current increased markedly with increasing negative *V*, while the half time, $t_{1/2}$, of current activations decreased (Fig. 2D). Upon returning *V* to the holding potential of +50 mV, currents decayed toward their prior steady-state level. Substituting mucosal Cl^- with gluconate (Fig. 2C) eliminated the time-dependent activations. Fig. 2E shows the steady-state currents as a function of transepithelial clamping potential. A strong degree of outward rectification characterises these currents. This rectification is manifested in the inverse S-shaped relationship between the steady-state conductance and *V* (Fig. 2F) showing that G_{Cl} is maximally activated at

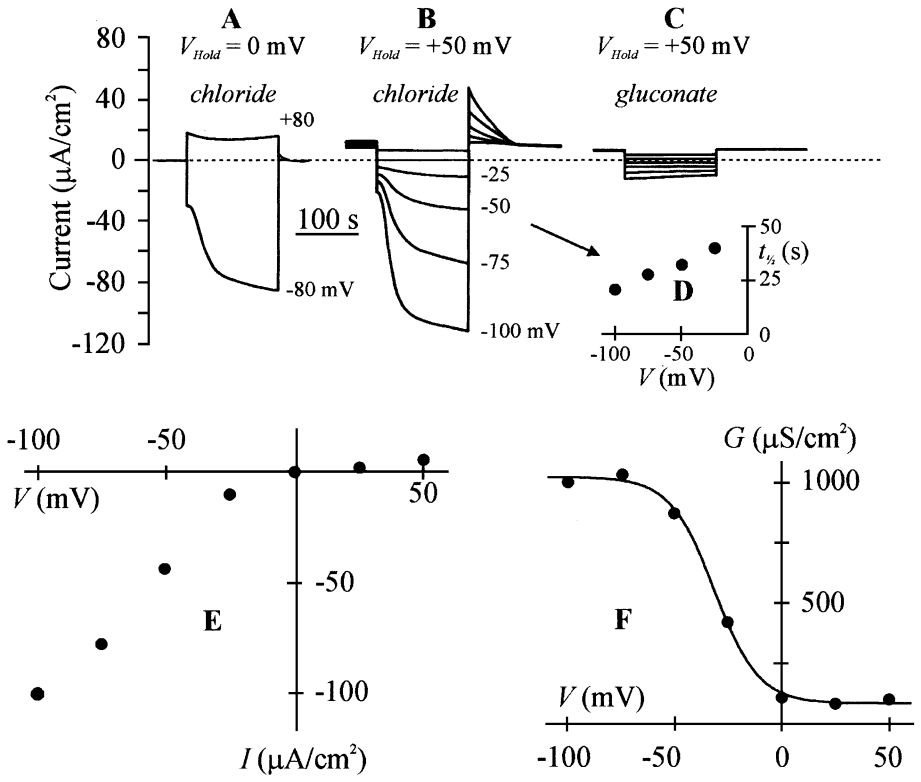

Fig. 2. Experimental protocols for studies on the chloride conductance of mr cells involve voltage clamping of the transepithelial electrical potential difference, *V*. Here and in all subsequent figures, *V* is referenced with respect to the grounded serosal solution. (A) Transepithelial current response to step change of *V* from a holding value of 0 mV to +80 and −80 mV, and back. The about 50-μm-thick epithelium was isolated by collagenase and mounted in an Ussing chamber with Na^+–Ringer's on the serosal side and K^+–Ringer's on the outside. As the outer surface of the epithelium has a very low K^+ permeability, the transepithelial electrical conductance is governed by the permeability to Cl^- [13]. Clamping of *V* in the physiological region ($V<0$ mV) reversibly activates chloride channels, which allows Cl^- to flow from the outer solution into the serosal bath. Note the dual role of the transepithelial electrical potential difference: (i) in a polarized fashion, *V* gates chloride channels, and (ii) drives Cl^- through the gated pathway. (B) The current response to voltage clamping depends on the anion present in the external solution. *V* was pulsed from a holding potential of +50 to −100 mV in steps of +25 mV. (C) Cl^- of the external bath was replaced by gluconate, and the *V*-pulse program repeated. With gluconate, the slow time-dependent activations are eliminated. (D) The half time ($t_{1/2}$) of the Cl^--conductance activation decreases with decreasing *V*. Generally, the 'gating' is slow, with half times in the order of 10–50 s. (E) The steady-state currents (obtained by a protocol depicted in B) are strongly rectified with large components in the physiological range of *V*. In this region, the current, *I*, is carried by an inward flow of Cl^-. (F) The gating of chloride channels results in an 'inverse S-shaped' conductance–voltage relationship of the epithelium. Typically, the conductance, *G*, saturates in the range, $-120<V<-80$ mV (i.e., the Cl^- conductance is fully activated). The line is the best fit to the Boltzmann distribution:

$$G = \frac{G_{max} - G_{min}}{1 - \exp[(V - V_0)/\Delta V]} + G_{min},$$

with $G_{max} = 1025 \pm 21$ μS/cm², $G_{min} = 89 \pm 17$ μS/cm², $V_0 = -32 \pm 1.4$ mV, $\Delta V = 10.5 \pm 1.2$ mV, $R^2 = 0.998$, and errors given for each of the free parameters. The fit was obtained by the Simplex routine of Origin© version 7 (Unpublished).

$V<-80$ mV. Since the large negative I_{Cl} is carried by a net influx of Cl^-, the physiological significance of this regulation is that chloride channels are activated only if the electrical driving force favours uptake of Cl^-. The fully activated currents (recorded at −100 mV) were found to be proportional to the density of mr cells (see Fig. 3) [13], which confirmed the hypothesis that the mr cells are the site of the chloride shunt as originally suggested in studies of frog skin [31,32]. Measurements of the volume response of single mr cells in situ using Kenneth Spring's method of video-enhanced quantitative microscopy added strong evidence that a component of the voltage-activated I_{Cl} flows through mr cells in both frog and toad skin [33,34].

2.2. Electrophysiological studies of isolated mr cells

Subsequent whole-cell [35] and single-channel [36,37] analyses of isolated mr cells showed that this cell type expresses Cl^- channels with depolarisation-activated Cl^- channels in the apical membrane (see below). However, as the fully activated membrane Cl^- conductance as well as the estimated single-channel activity could not account for the macroscopic currents measured in the intact epithelium, it was hypothesised that the voltage-activated I_{Cl} flows through an ion-selective pathway associated with tight junctions [38,39]. We addressed this question by single-cell voltage-clamp experiments by a method originally intro-

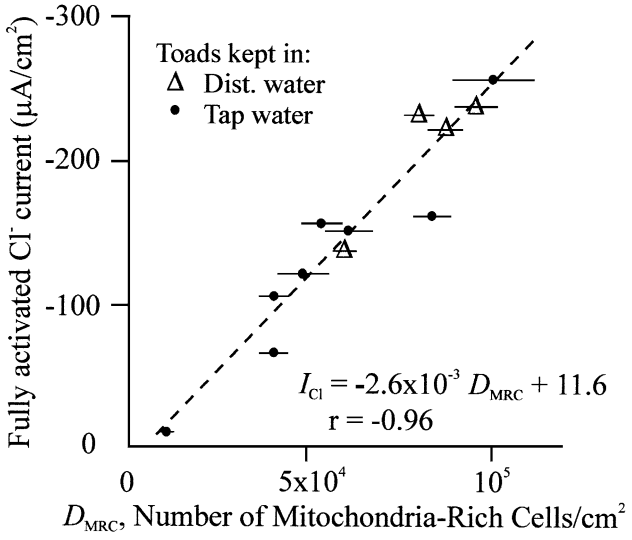

Fig. 3. The linear relationship of toad skin epithelium between density of mr cells, D_{MRC}, and fully activated chloride current measured at a transepithelial potential difference of − 100 mV. The slope of the regression line indicates that, on average, a single mr cell contributes with a current of − 2.6 nA at V = − 100 mV. Modified from Ref. [13].

duced for studies of retinal rod cells [40], in which a pipette serves as a micro-Ussing chamber [41] (see Fig. 4A). With this method, the putative dynamic conductance of single mr cells can be studied by patch-clamp technology using a preamplifier of low feedback resistance.[2] With Ringer's solutions in both bath and pipette [41], V_P was pulsed from a holding value of + 100 to − 100 mV (Fig. 4B). Before the voltage pulse, the holding current was 2.42 nA (V_P=+100 mV), and 'instantaneously' the current reversed to − 2.46 nA when V_P was shifted to − 100 mV. This 'ohmic' current can be assumed to flow through the seal between the cell and the glass wall, that is, with a leak conductance of 24.4 nS. Subsequently, the pipette current was slowly activated, and with a half time of ~ 24 s, the current reached a new steady-state value of − 3.45 nA. Upon return of V_P to + 100 mV, the current returned to its prepulse value (2.37 nA). A family of such currents was recorded at different V_P values (Fig. 5A). The half time of current transients of the single mr cell decreased with decreasing clamping potential (see Fig. 5B), as is the case for the macroscopic currents in Fig. 2. The steady-state currents obtained from a single mr cell with the leak currents subtracted are summarised in Fig. 5C. A strong outward rectification is apparent. Like the macroscopic Cl^- conductance of the intact epithelium, also the single-cell conductance, G, is activated by V_P along an inverse S-shaped relationship that saturates for $V_P \approx -100$ 100 mV (Fig. 5D). Table 1 collects the results of this type of experiments for comparing the estimates of the fully activated I_{Cl} and G_{Cl} with those obtained in previous studies using other methods. Independent of method, it is obvious that the estimated chloride currents imply that the activated mr cell displays a significant chloride conductance, and that the single-cell estimates account for the transepithelial conductance. Thus, with a G_{Cl} of 10–100 nS/cell (Table 1) and 50,000 mr cells/cm^2 [13], the conductance of the transepithelial chloride shunt of the intact epithelium would be about 0.5–5 mS/cm^2, that is, a range covering measured values (cf. Fig. 2F). Interestingly, the amplitude of the Cl^- current seems affected by the superfusion of the cell with oxygenated Ringer's solution during the recording. Thus, in 16 non-perfused cells, the activated current was − 2.90 ± 0.48 nA at V_P = − 100 mV (exemplified in Fig. 4) as compared to 10 perfused cells with a steady-state activated current of − 7.99 ± 1.48 nA recorded at a similar V_P (exemplified in Fig. 5). In the two groups, the currents ranged from − 1.0 to − 7.6 nA and from − 3.3 to − 14.4 nA, respectively, with the two means not being statistically different (P>0.36). It is noteworthy, though, that the single-cell current estimated in 'in situ studies' falls within the lower range of values of the directly recorded currents (non-perfused isolated cells, Table 1).

2.3. Dependence on oxidative energy metabolism

Flux-ratio analysis showed that the chloride ions flow through the voltage-activated conductance by electrodiffusion [13]. Nevertheless, soon after the voltage-sensitive chloride conductance was discovered [43], it was observed that I_{Cl} is strongly dependent on the energy metabolism of the epithelium [44]. This is illustrated in Fig. 6A, which shows that brief exposure to an O_2-free solution leads to a reversible inactivation of the Cl^- conductance. A similar effect is seen if the metabolic inhibitor cyanide is added to the external bath (Fig. 6B). These results seem to imply that the activity of the Cl^- channels is regulated via metabolically (ATP) dependent signalling pathways. Nagel and Katz [45] also found that addition of cyanide as well as the uncoupler of oxidative phosphorylation, dinitrophenol, inhibits the voltage-activated chloride current. However, unlike our experiments that always showed significant inhibition of the Cl^- current to exposure of an O_2-free, N_2-equilibrated Ringer's solution (Fig. 5A), this treatment had no effect in their experiments [45]. They suggested, therefore, that the cyanide effect is not due to inhibition of cellular energy metabolism, but reflects an anion-dependent inhibition either of the activation mechanism or the channel. Their hypothesis and ours are not mutually exclusive, and as we will discuss below, there is strong evidence that binding of anions to external bindings sites interferes with the activity of the chloride channels.

[2] Isolated mr cells are prepared by trypsin or pronase treatment of the epithelium [35]. During the separation of mr cells, the preparation is bathed in nominally Ca^{2+}-free solutions, but with no chelator added, which maintains sufficient enzyme activity. In the presence of Ca^{2+} in the millimolar range, the voltage-activated chloride conductance of the intact tissue is inhibited by trypsin added to the serosal bath. The chloride conductance was not fully recovered after washout of the enzyme [42].

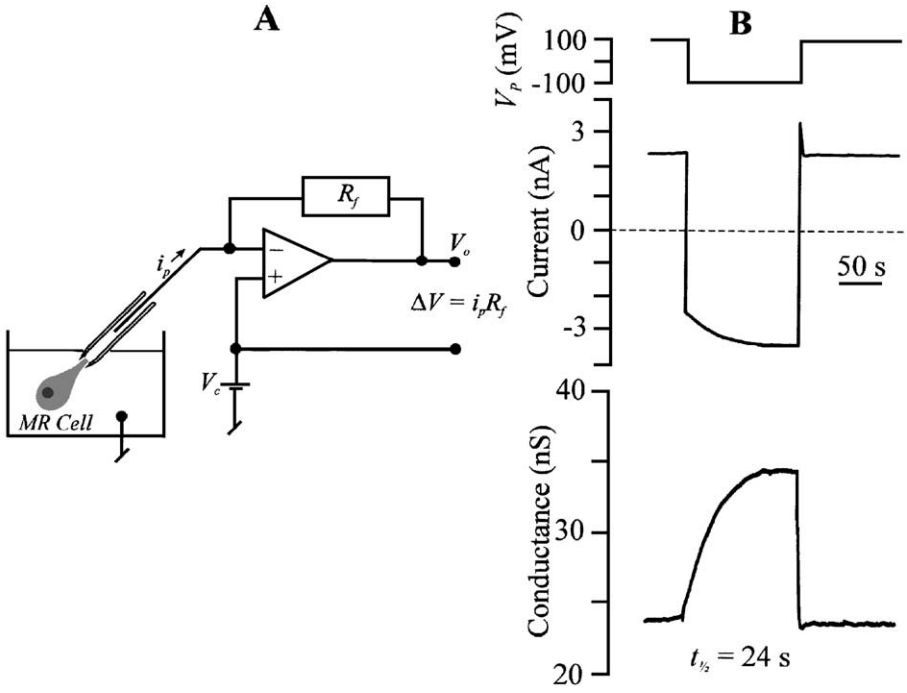

Fig. 4. The electrophysiology of single mr cells studied by a modified 'patch-clamp' technique. (A) The neck of the mr cell is gently sucked into the tip of a specially designed patch pipette. With grounded bath, the pipette potential, V_P, is the transcellular electrical potential difference. The pipette current, i_p, flows through the cell and between the neck of the cell and the wall of the pipette, and is recorded with a fairly small feedback resistor of the patch-clamp pre-amplifier (50–100 MΩ, Ref. [41]). (B) In this configuration, the cell can be studied by a protocol similar to that applied to the intact epithelium (cf. Fig. 2). (Upper panel) From a holding value of +100 mV, V_P was pulsed for 150 s to −100 mV, and back. (Middle panel) The current response contains a relatively large ohmic component, which is associated with a 'seal resistance' of about 40 MΩ, and a slow dynamic component of about −1.1 nA. (Lower panel) Time course of the calculated conductance response of the cell. The fully activated dynamic conductance is 11 nS (#AU2996AD, unpublished from Ref. [41]).

2.4. External [Cl^-] dependence: activation and self-inhibition

In the study leading to the two-membrane hypothesis, Koefoed-Johnsen and Ussing [46] eliminated the conductive chloride permeability by exposing the outside of the skin to a Ringer's solution in which [Cl^-] was diluted ×100. Experiments by Kirschner [27] indicated that the passive Cl^- conductance is fully downregulated at a few millimolar Cl^-. In frog skin, the ranking of anions capable of keeping the anion conductance activated, $Cl^- > Br^- \gg I^-$, is different from the ranking of the anion permeability of the activated pathway, $SCN^-:Br^-:Cl^-:I^- = 1.8:1.3:1:0.8$. Thus, it was suggested that an external binding site for Cl^-, different from the translocation site of the activated channel, opens the channel when occupied by Cl^- [47]. The concentration dependence of this process was studied in more detail in experiments with toad skin [48]. In this preparation, the voltage-activated anion currents indicated a ranking of $I_{Cl} > I_{Br} \gg I_I > I_{gluconate}$ (Fig. 7A). This ranking, like that of frog skin, is a measure of the regulation via putative external regulatory sites rather than a consequence of the anion selectivity of the activated conductance pathway. This point is logically inferred from the following results. The chloride influx, J_{Cl}^{in}, through the voltage-activated conductance of mr cells, increases along an S-shaped curve with external [Cl^-] and saturates at high concentrations (Fig. 7B). Simultaneous measurements of J_I^{in} (with $^{124}I^-$, Fig. 7C-a) and J_{Cl}^{in} (with $^{36}Cl^-$, Fig. 7C-b) in experiments with constant (low) external [I^-] and varying external [Cl^-] showed that the permeability of the ions exhibits similar $[Cl^-]_o$ dependence with a ratio of $P_I/P_{Cl} \approx 0.7$ (compare right-hand axes of Fig. 7C-a,b). This poor selectivity of the voltage-activated anion channel is independent of the external Cl^- concentration (1.45 mM ≤ $[Cl^-]_o$ ≤ 110 mM, cf. Fig. 7C). The analysis was extend to cover Br^- as well, and with Ringer's solution outside and $V = -80$ mV, the following ranking was obtained: $P_{Br}:P_{Cl}:P_I = 1.31 \pm 0.03:1:0.73 \pm 0.05$ [48]. Thus, while the activated anion conductance exhibits weak anion selectivity (as revealed by permeability coefficients calculated from isotope fluxes, Fig. 7C), the affinity of the regulatory binding site(s) is strongly dependent on the identity of the anion (as revealed by the current response to external anion substitutions, Fig. 7A). The dependence of the voltage-activated chloride conductance on the external anion is somewhat more complicated. While external Cl^- in the range 1.45 mM < $[Cl^-]_o$ < 60 mM increases the

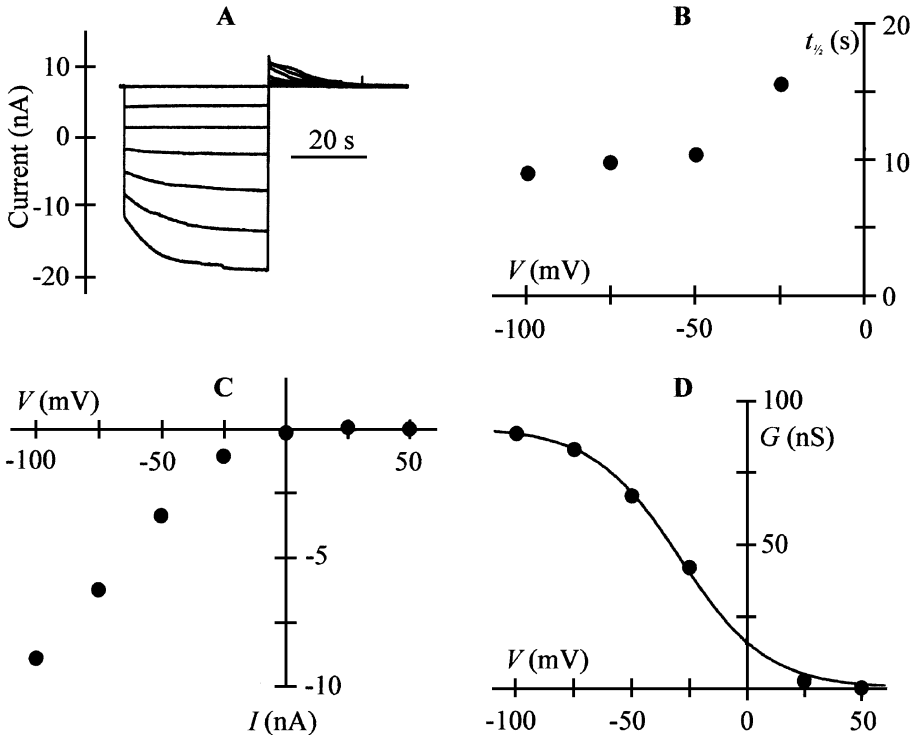

Fig. 5. Transcellular voltage clamp of single mr cell. (A) Family of pipette currents obtained by 40-s pulses of V_P from a holding potential of +50 mV to voltages between −100 and +25 mV in steps of +25 mV. The currents contain an ohmic and a dynamic component. (B) The half time of the dynamic component, $t_{1/2}$, is in the order of 10 s and is decreasing with decreasing clamping voltage. (C) Voltage dependence of the steady-state dynamic currents recorded in panel A. (D) Voltage dependence of the dynamic conductance of the mr cell. The line is the best fit to the Boltzmann distribution:

$$G = \frac{G_{max} - G_{min}}{1 - \exp[(V - V_0)/\Delta V]} + G_{min},$$

with $G_{max} = 90 \pm 2$ nS, $G_{min} = 0.02 \pm 2.3$ nS, $V_0 = -27 \pm 2$ mV, $\Delta V = 18.3 \pm 2.6$ mV, $R^2 = 0.999$, and errors given for each of the free parameters. The fit was obtained by the Simplex routine of Origin© version 7. Note the similarity with the intact epithelium (Fig. 2) of the steady-state current–voltage relationship as well as of the conductance–voltage relationship (unpublished figure from Ref. [41]).

macroscopic permeability (i.e., very likely, activates channels), the permeability decreases again with a further increase of $[Cl^-]_o$ (see Fig. 7C). According to this interpretation, the saturation shown in Fig. 7B is accounted for by self-inhibition. Results of a more detailed study indicated that I^- inhibits the anion conductance at much lower concentrations than Cl^- and Br^- [48].

2.5. Patch-clamp studies of the voltage-controlled Cl^- conductance

Patch-clamp studies have been carried out with isolated mr cells of the toad skin epithelium. With 100 μM amiloride and 5 mM Ba^{2+} added to the bath, and 10 mM Cs^+ in the pipette-solution, whole-cell currents reversed at E_{Cl} showing that with this protocol, the membrane current is carried by Cl^- [35]. The conductance–voltage relationship of an isolated mr cell in whole-cell configuration is shown in Fig. 8A. The membrane's Cl^- conductance increases with depolarizing voltage as would be expected if the voltage-activated Cl^- channels are located in the apical membrane.[3] The chloride conductance is about half-maximally activated at a membrane potential of +25 mV, that is, at this pipette potential, the open probability of gated channels is $P_O \approx 0.5$, with the variance of stationary current fluctuations being maximal. In Fig. 8B are shown whole-cell currents recorded at three different pipette potentials, +25 mV (Cl^- conductance half-maximally activated), E_{Cl} (no current flowing through Cl^- channels), and −75 mV (Cl^- conductance deactivated), respectively. Activation of the steady-state Cl^- current from −90 pA (−75 mV) to 314 pA (+25 mV) was associated with a large increase in the variance of the current fluctuations about its stationary mean value from $\sigma^2 = 49 \pm 1$ pA^2 ($V_P = -75$ mV) to $\sigma^2 = 889 \pm 10$ pA^2 ($V_P = +25$ mV). The power density spectrum of current fluctuations recorded at $V_P = +25$ mV shown in Fig. 8C contains a single Lorentzian component, $S(f) = S_0/[1 + f^2/f_C^2]$, with $S_0 = 11.7 \pm 0.5$ pA^2 and $f_C = 41.3 \pm 2.7$ Hz. The following set of equations governs the relationship

[3] It is noted that transcellular hyperpolarisation results in a depolarisation of the apical membrane and a hyperpolarisation of the basolateral membrane.

Table 1
The fully voltage-activated transcellular Cl^- conductance of a single mr cell as estimated by different methods

Method	I_{Cl} ($V=-100$ mV) (nA/cell)	G_{Cl}^{max} (nS/cell)	Protocol	Ref.
Slope of $I_{Cl}-D_{MRC}$ relationship	-2.6 ($n=12$, $r=-0.96$)	26	*B. bufo* in situ	[13]
Self-referencing voltage probe (*Salt adapted frogs*)	-1.2 ($n=15$)	12	*Rana pipiens* in situ	[33]
$\Delta I_{Cl}/\Delta D_{MRC}$ (*Aqua distilled adapted*)	-2.0 ($n=5$)	20	*B. bufo* in situ	[24]
Single-cell voltage clamp (*Non-perfused*)	-2.90 ± 0.48 ($n=16$)	29	*B. bufo* trypsin	[41]
Single-cell voltage clamp (*Non-perfused*)	-2.14 ± 0.72 ($n=5$)	21	*B. bufo* pronase	[41]
Single-cell voltage clamp [*Perfused* ($t_{1/2}\approx3$ s)]	-7.99 ± 1.48 ($n=10$)	80	*B. bufo* trypsin	[41]

I_{Cl} = transcellular current at a transcellular electrical potential difference of -100 mV (serosal side grounded).

between open channel probability (P_O), single-channel current (i_{Cl}), single-channel conductance (γ_{Cl}), macroscopic mean current (I_{Cl}), variance (σ^2), and the parameters of the Lorentz spectrum (S_0 and f_C):[4]

$$I_{Cl} = i_{Cl}P_O N \quad (1)$$

$$i_{Cl} = \frac{\sigma^2}{I_{Cl}(1-P_O)} \quad (2)$$

$$\sigma^2 = \frac{\pi S_0 f_C}{2} \quad (3)$$

$$\gamma_{Cl} = \frac{i_{Cl}}{V-E_{Cl}} \quad (4)$$

With the observed variables discussed above, the single-channel conductance was estimated to be in the range of 150–300 pS [35]. The interpretation of the analysis, however, is not straightforward. With a corner frequency of 40 Hz, the time constant of the above fluctuations is 4 ms, which is very fast as compared to the slow activation of transcellular Cl^- currents (cf. Figs. 2, 4 and 5). Furthermore, the Cl^- current rectification in whole-cell mode was nearly instantaneous, with only few cells exhibiting current activations with a long time constant, and still other cells exhibiting no voltage activation at all [35]. This might be interpreted to mean that we are dealing with two different processes, (i) a slow activation requiring an intact submembrane domain, which is vulnerable to the invasive whole-cell configuration, and (ii) stationary fluctuations due to spontaneous opening and shutting of channels residing in the membrane. Being no more than a speculative possibility at this stage of the analysis, the general conclusion is that the mechanism of the dynamic behaviour of the chloride current through the apical membrane of mr cells is poorly understood.

[4] Noise analysis of voltage-activated channels is usually carried out by construction of Sigworth plots of current activations [49]. With a half time of current activation of 20 s, or more (Figs. 2–4), such an analysis would require reproducible membrane currents for a period of more than 40 min (20 records of at least 120 s each), which is not possible. Thus, it was attempted to carry out an analysis of stationary currents in whole-cell configuration, which turned out to be governed by much faster rate constants.

In a direct study, chloride channels of the apical membrane of mr cells have been resolved, and based upon the single-channel conductance and current–voltage relationships, several types of Cl^- selective channels were identified [36]. Only a few percentage of the sealed patches displayed the predicted large-conductance voltage-activated Cl^- channel, and one example is shown in Fig. 8D. Typically, the channel exhibits substates and stepwise openings and closures as well as transitions in one go between the open and closed states. It may not be surprising that this

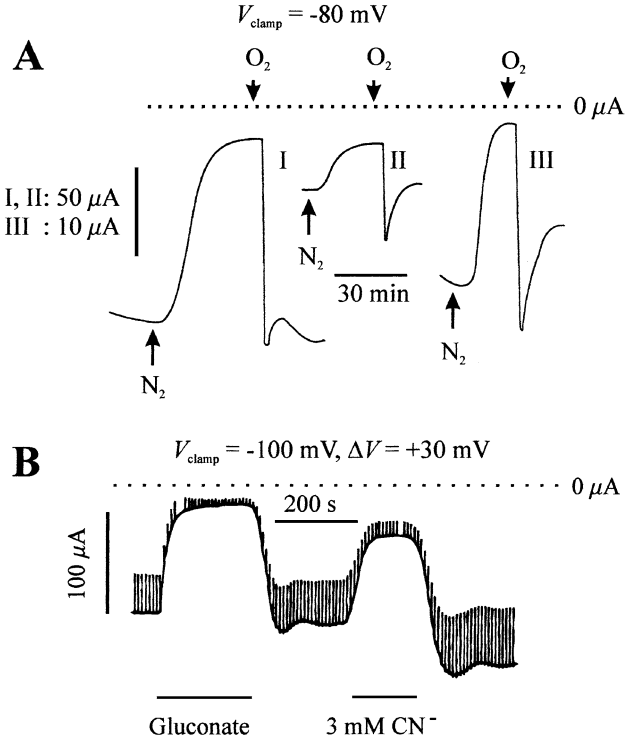

Fig. 6. (A) The voltage-activated I_{Cl} of toad skin epithelium is strongly dependent on the supply of oxygen to the preparation [44]. The three examples shown are from three different preparations (I, II, and III, respectively) mounted in a closed Ussing chamber and gassed with atmospheric air ('O_2') and N_2, respectively. The onset of current inhibition is slow and fully reversible. Note the fast recovery with 'overshoot' following reintroduction of atmospheric air. (B) Toad skin epithelium clamped at -100 mV where the major fraction of the current is carried by an inward flux of Cl^- (as seen from the response to substitution of external Cl^- by gluconate). Addition of 3 mM CN^- to the solution bathing the outside of the preparation results in a similar decrease of the chloride current. Also shown are the current responses to 1 s transepithelial current pulses of +30 mV amplitude (unpublished recordings from Ref. [44]).

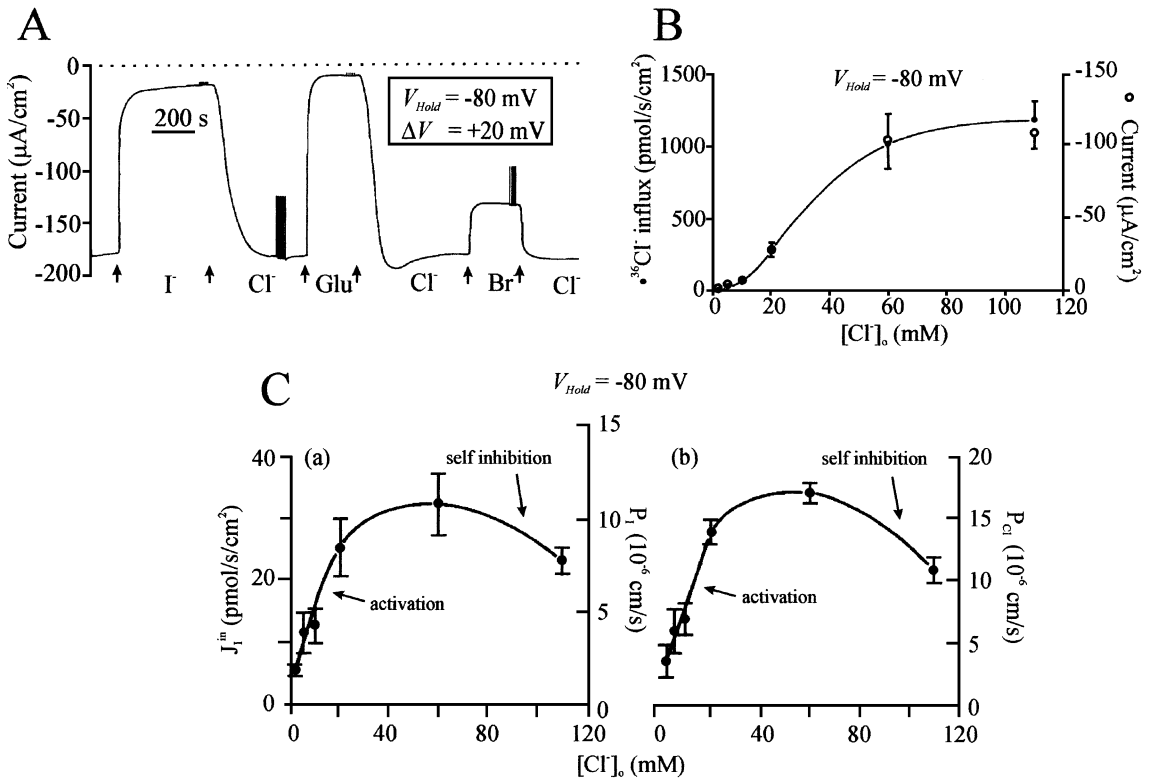

Fig. 7. Concentration dependence of the chloride permeability of mr cells (modified from Ref. [48]). (A) With NaCl–Ringer's inside and KCl–Ringer's outside, the chloride permeability was activated by clamping the transepithelial potential difference to −80 mV. Shown are the transcellular current responses to reversible replacement of external Cl^- with I^-, gluconate, and Br^-, respectively. (B) (Closed symbols) The steady-state unidirectional influx of Cl^- decreases along an S-shaped curve with decreasing external chloride concentration, $[Cl^-]_o$. Gluconate was substituted for chloride. (Open symbols) At all concentrations, the influx constituted the major component of the transepithelial current (the current scale on the right-hand side is equal to the flux scale on the left-hand side multiplied by the Faraday). For both relationships are shown means ± 1 S.E. (C) The unidirectional iodide influx was measured in the same preparations, but with the external iodide concentration held constant, $[I^-]_o = 3$ mM. Since I^- permeates the chloride channels, with this protocol, the I^- influx reveals the activation and self-inhibition of the anion permeability with increasing $[Cl^-]_o$. The permeability coefficients were calculated as, $P_I = ((J_I^{in})/([I^-]_o))$ and $P_{Cl} = ((J_I^{in})/([Cl^-]_o))$, respectively ($V = -80$ mV).

kinetically complicated channel rarely is resolved. Considering a fully activated conductance of 40 nS/cell (Figs. 4 and 5 and Table 1) and an apical membrane area of circa 4 μm^2 (Fig. 1), the specific cell conductance is about 1000 mS/cm^2 (disregarding microplicae). This estimate corresponds to more than 40 *V*-activated Cl^- channels per square micrometers. A membrane with such a high density of channels is not easy to study at a single-channel level.

3. The receptor-activated Cl^- conductance of mr cells: CFTR

3.1. Selectivity and pharmacology of the isoproterenol-activated conductance

In the isolated epithelium treated with amiloride to eliminate the active Na^+ current, application of β-adrenergic agents, like isoproterenol, increased G_{Cl} several fold, while the apical membrane of principal cells remained literally tight to Cl^- [30]. Isoproterenol acts via a membrane-bound receptor that activates the adenylate cyclase leading to the formation of cyclic AMP (cAMP) from ATP. cAMP activates protein kinase A, which by phosphorylation, leads to activation of the G_{Cl}. The cascade could also be initiated at the level of the adenylate cyclase (forskolin) or by directly adding a membrane permeating cAMP analogue (dibutyryl- or 2-chlorophenylthio-cAMP) to the isolated epithelium [30,50–52]. Fig. 9 shows the results from an experiment with an isolated epithelium mounted in an Ussing chamber and stimulated by isoproterenol. With the active transport of Na^+ eliminated and subepidermal glands absent, the conductance increased to about 10 times above its resting value, while the current (recorded at $V = 0$ mV) remained close to zero. Thus, unlike stimulation by this agonist of acinar cells of exocrine glands, in the absorbing skin epithelium, the activated conductance mediates a passive flux of Cl^- through the responding cells, which were shown not to be the principal cells [30]. Substitution of external Cl^- with other halide ions showed that both I^- and Br^- pass the activated conductance pathway (Fig. 9). With this protocol, the following ranking of conductances was obtained [53]: $G_{Cl}:G_{Br}:G_{NO_3}:G_I:G_{gluconate} = 1:0.75\ (\pm 0.03):0.68\ (\pm 0.11):0.38\ (\pm 0.03):0.25\ (\pm 0.02)$, where the conduc-

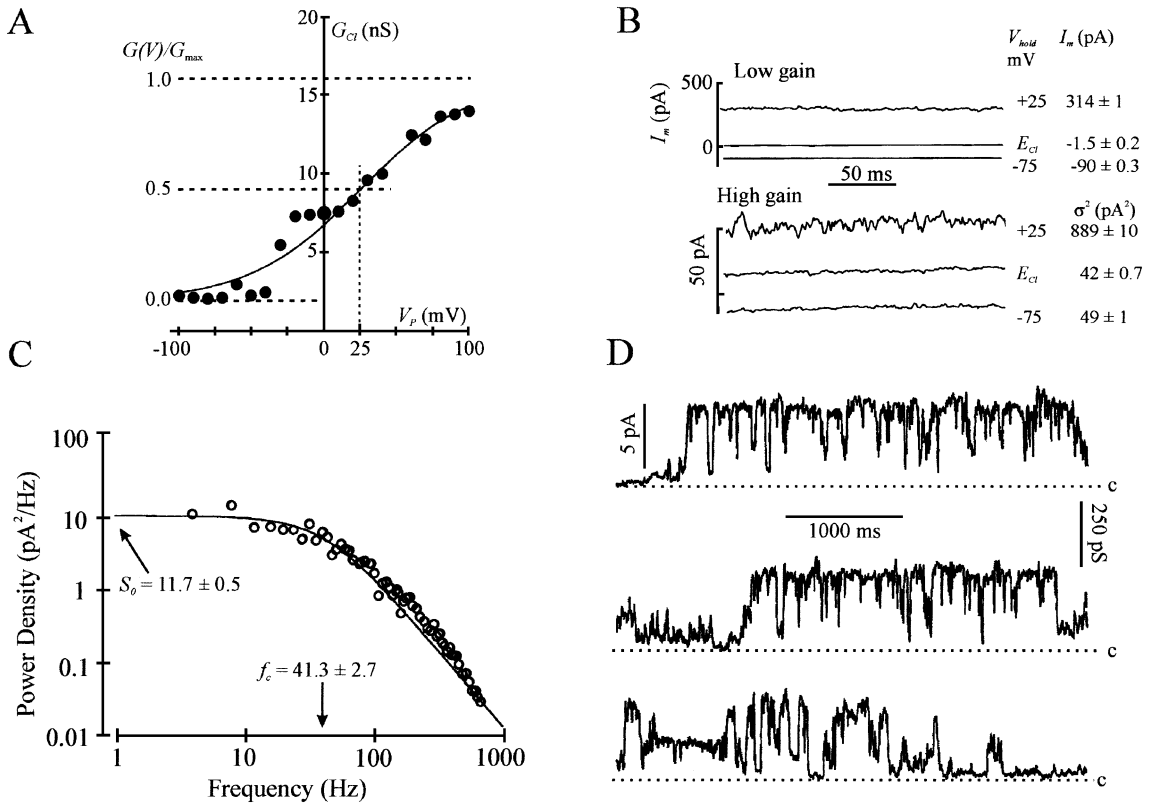

Fig. 8. Estimates of the conductance of the voltage-activated apical channels of mr cells. (A) Conductance–voltage relationship of isolated mr cell in whole-cell configuration with cation channels blocked. (B) Stationary whole-cell currents of a mr cell. (Upper panel) Membrane current at three different pipette potentials, +25 mV (Cl^- conductance activated), E_{Cl}, and −75 mV (Cl^- conductance deactivated), respectively. (Lower panel) Same currents as above but recorded at 10 times higher gain and with d.c. component subtracted. (C) Power density spectrum of current fluctuations recorded at V_P=+25 mV ('background spectrum' subtracted [35]). The line is the best fit to a single Lorentzian given by, $S(f)=((S_0)/([1+f^2/f_C^2]))$, with $S_0=11.7\pm0.5$ pA^2 and $f_C=41.3\pm2.7$ Hz. (D) Single-channel activity of voltage-activated apical chloride channel. Ten seconds continuous recording from a cell attached patch at $-V_P$=+20 mV and with Ringer's solution in bath and pipette. 'C' indicates current level with channels closed. Note that in the cell attached configuration, $-V_P$=20 mV corresponds to V_P=20 mV in the 'whole-cell' configuration of panel A. That is, at this potential, the population of chloride channels would be expected to be half maximally activated. Recordings given in panels A, B, and C are modified from Ref. [35], and that of panel D from Refs. [28,36].

tance with gluconate outside is not significantly different from the control conductance of the non-activated preparation ($G_{control}-G_{gluconate}=87\pm65$ μS/cm^2, $P=0.21$). This sequence of relative conductances is similar to that of human cystic fibrosis transmembrane conductance regulator (CFTR) heterologously expressed in *Xenopus* oocytes [54,55].

Like the CFTR-mediated apical chloride conductance of human epithelia, which is also under the control of β-adrenergic receptors, the agonist-activated Cl^- conductance of the amphibian epithelium was stimulated by external application of 50 μM genistein (mean ± S.E., number of preparations), $G_{control}=194\pm38$ μS/cm^2, $G_{isoproterenol}=1290\pm271$ μS/cm^2, $G_{genistein}=2021\pm492$ μS/cm^2, $n=6$ (for the genistein effect, $P<0.013$, paired *t*-test). As further evidence for the functional expression of the amphibian CFTR gene, the activated Cl^- conductance was slowly inhibited by adding 200 μM of the *h*CFTR-inhibitor glibenclamide to the serosal bath, $G_{control}=271\pm40$ μS/cm^2, $G_{isoproterenol}=1973\pm142$ μS/cm^2, $G_{glibenclamide}=631\pm116$ μS/cm^2, $n=6$ ($P<10^{-4}$) [unpublished results].

In a study of isolated epithelia of frogs (*Rana temporaria*, *Rana esculenta*) and toads (*Bufo viridis*, *Bufo regularis*), Nagel and Katz [56] showed that stimulation of an α_1-adrenergic receptor inhibited the activated chloride conductance. They suggested that this receptor regulates the voltage-activated chloride conductance via the cytoplasmic [Ca^{2+}]. Thus, it appears that β-adrenergic as well as the α_1-adrenergic receptor are expressed on the basolateral membrane of the mr cell type.

3.2. Single-channel studies

The apical plasma membrane of mr cells expresses a small conductance Cl^--specific channel, which occurred more frequently in cells pre-treated with forskolin as compared to non-treated control cells [36]. As an example, Fig. 10 shows currents recorded from an inside-out patch. With symmetrical [Cl^-], the currents reversed near 0 mV, that is, close to E_{Cl} and far from the equilibrium potential of the major diffusible cation, $E_{Na}=-79$ mV. The slope of the

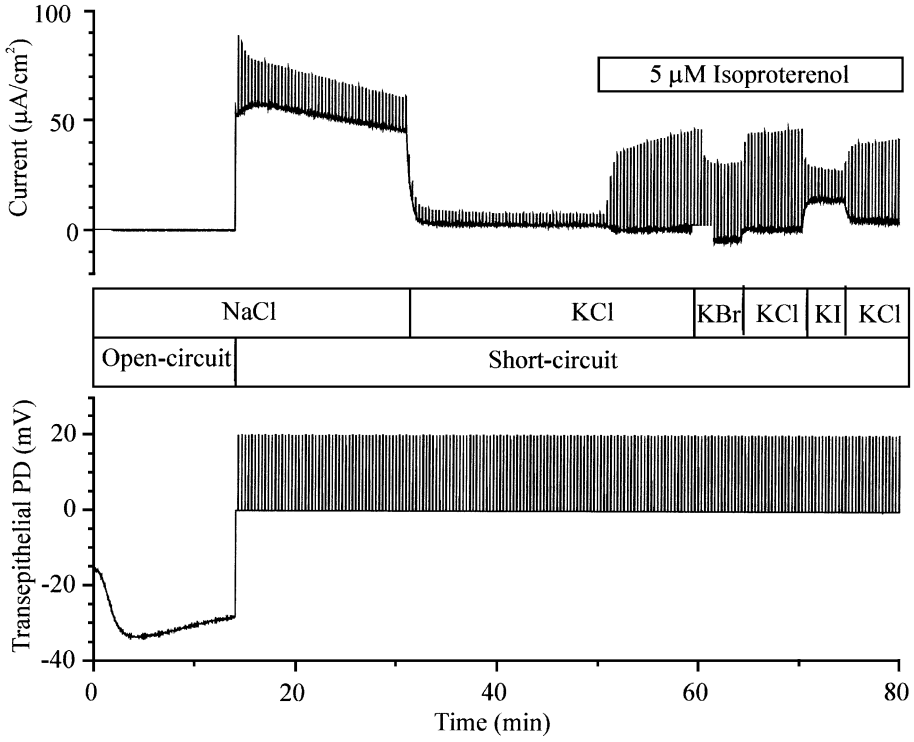

Fig. 9. Bioelectric response of the isolated epithelium to activation via β-adrenergic receptors of the putative toad *bb*CFTR. Initially, the isolated epithelium was exposed to NaCl–Ringer's on both sides under open circuit condition. Subsequently, the preparation was short-circuited for monitoring the active Na^+ current. Half an hour after mounting of the epithelium in the Ussing chamber, the external sodium ions were replaced by potassium ions, whereby the inward current dropped from 45 to 2.7 μA/cm^2, which was associated with a conductance decrease from 790 to 260 μS/cm^2. Serosal application of 5 μM isoproterenol resulted in stimulation of the transepithelial conductance to about 2245 μS/cm^2. Substitutions of external Cl^- with other halide ions revealed a ranking of permeabilities of $P_{Cl}>P_{Br}>P_I$ (unpublished).

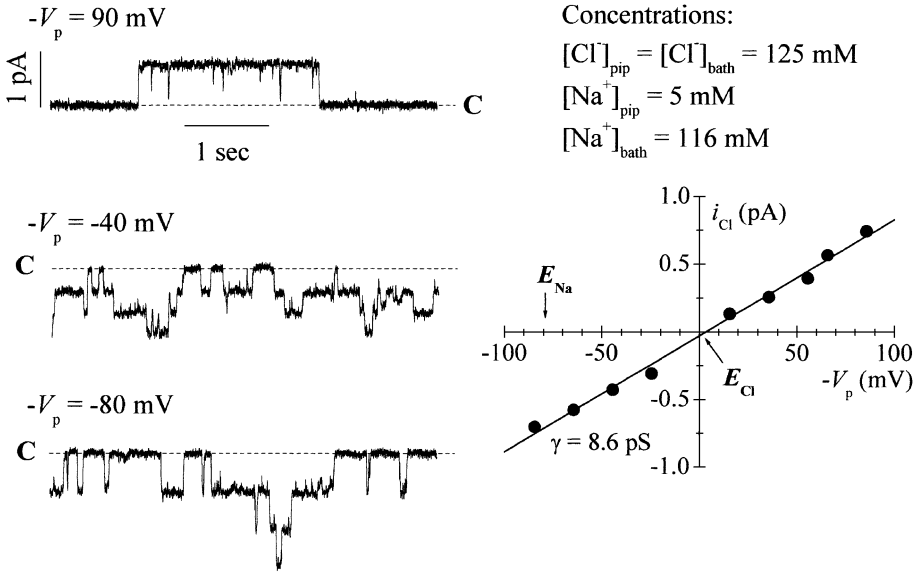

Fig. 10. Single-channel recording of inside-out patch from apical membrane of mr cells. (Left-hand panel) The patch contained at least three active channels here recorded at three different pipette potentials as indicated. 'C' indicates current level with all channels shut. (Right-hand panel) Single-channel current–voltage relationship with similar [Cl^-] in bath and pipette, but with different cation concentrations as indicated. The limiting conductance, $\gamma_{125/125}=8.6$ pS together with the immunocytochemical verification of CFTR in the mr cell (Fig. 11B) would indicate that this channel is the amphibian homologue of human CFTR, but—as explained in the text—the definitive electrophysiological proof was not obtained [28,36].

i_{Cl}–V relationship corresponds to a conductance of 8.6 pS ($\gamma_{125/125} = 7.1 \pm 0.5$ pS, $n = 11$). Taken together, these observations would indicate that the channel is the toad's homologue of human CFTR. However, since the lifetime of patches containing this small-conductance channel was short, it was not possible to carry out halide selectivity studies. Nor was it possible to verify that the channel's activity depends on a combination of PKA phosphorylation

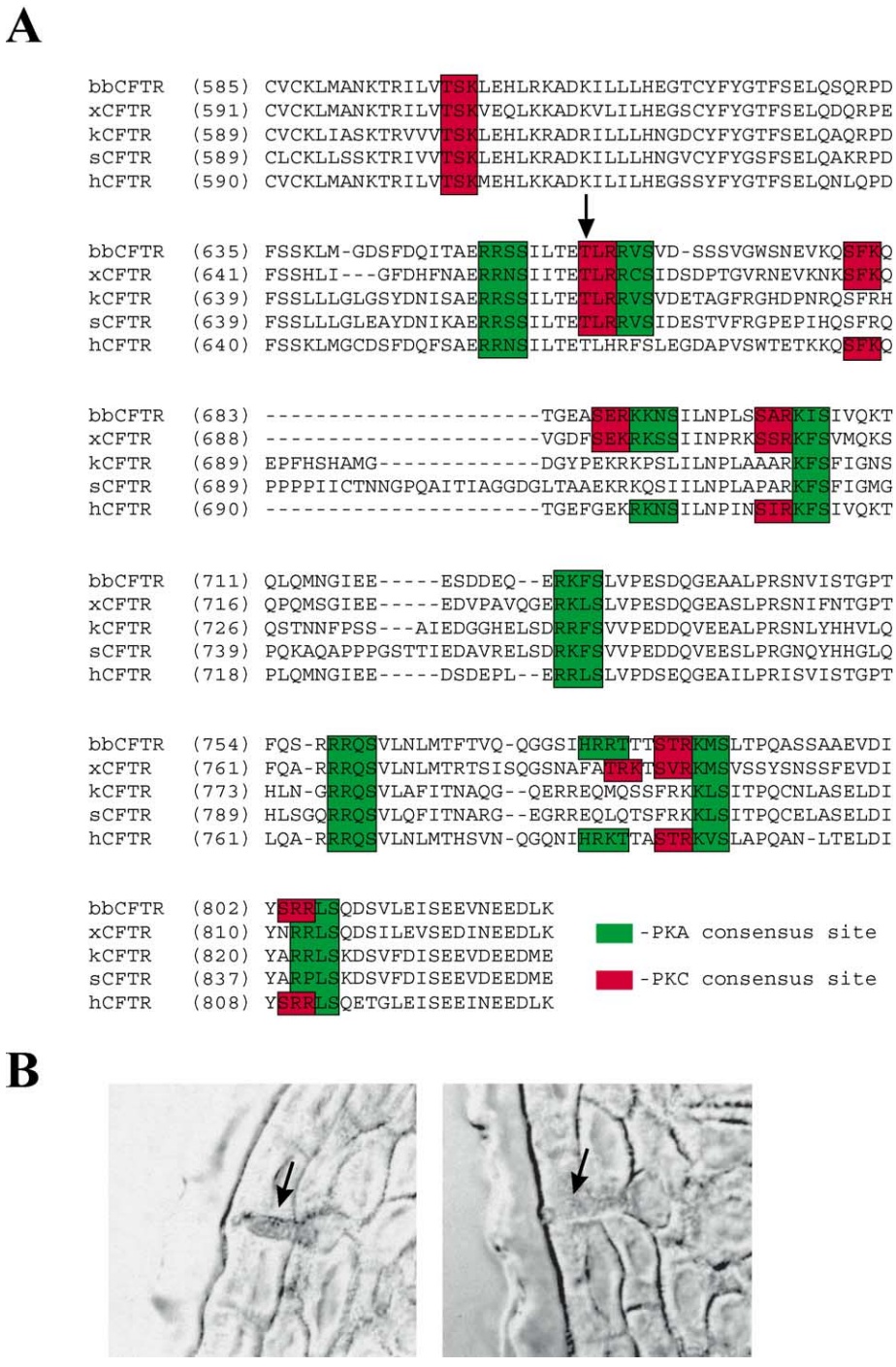

Fig. 11. (A) Alignment of the deduced amino acid sequence (VectorNTI Suite ver. 6.0™) of the R-domain of toad *bb*CFTR, *Xenopus x*CFTR, killifish *k*CFTR, *Salmo s*CFTR, and human *h*CFTR. Phosphorylation consensus sites are shown. Green box, PKA; red box, PKC. The arrow points at threonine residue of the PKC consensus site, which confers PKC activation of *x*CFTR as discovered in Ref. [61]. It is preserved in amphibian and teleost CFTR and is absent in *h*CFTR. (B) Immunohistochemical localization of CFTR in toad skin epithelium. A mixture of two anti-*h*CFTR antibodies specific for the C-terminus and the R-domain (R&D Systems, Cat. No. MAB25031 and MAB1660) was added to 5 μm paraffin sections. (Left-hand panel) Only the mr cell stains (arrow) with no reactions in principal cells. (Right-hand panel) Preparations to which the primary antibodies were not added, and which were treated only with the horseradish peroxidase-conjugated secondary antibody, did not stain. For methods, see Ref. [53].

of the R-domain and ATP hydrolysis at the NBD1 and NBD2 domains, which is the hallmark of *h*CFTR [57,58].

3.3. Molecular biology: expression and properties of a CFTR-channel protein

We therefore took a molecular biological approach for identifying the putative expression of CFTR in mr cells of *B. bufo*. RT-PCR on the skin epithelium with primers constructed from *Xenopus leavis* CFTR [59] gave a transcript of a size corresponding to the targeted region of the *x*CFTR gene [53]. With primers flanking three successive regions of the *x*CFTR cDNA (each of about 1500 bp length), full-length *bb*CFTR cDNA was cloned (GenBank AYO26761). Subsequent alignment of the derived protein with that of the cloned [60] *h*CFTR revealed an overall identity between *Bufo* and human CFTR of 89%. The two nucleotide binding domains (NBD1 and 2) are well conserved including identified Walker A and B motifs, ATP binding sites, and the ABC transporter signature of NBD1 [53]. As shown in Fig. 11A also, the R-domain of the cloned *bb*CFTR exhibits high degree of identity with that of other cloned vertebrate CFTR, which includes nine PKA- and seven PKC-consensus sites of this domain of the *Bufo* clone. Recently, it was discovered that *x*CFTR, unlike *h*CFTR, is equally well activated by PKC and PKA phosphorylation. Site-directed mutagenesis showed that the PKC consensus site at Thr^{663} of *x*CFTR, that is, Thr^{665} of *h*CFTR, is mandatory for this activation of the channel [61]. This site is preserved in *bb*CFTR and in the other cloned CFTR from lower vertebrates shown in Fig. 11A and indicated by the arrow with the sequences of *Salmo* and *Fundulus* taken from Refs. [62,63], respectively.

The cell type of the epithelium that expresses CFTR was localised by immunostaining with commercially available monoclonal antibodies raised against regions of the C-terminus and the R-domain of *h*CFTR, which are well preserved in *bb*CFTR [53]. Fig. 11B, left-hand panel, shows that the mr cells stain with this mixture of antibodies. No reaction is seen in principal cells, which do not display a cAMP-activated Cl^- conductance [30], nor are mr cells stained with only secondary antibody present (Fig. 11B, right-hand panel).

4. Cytochalasin D removes deactivation

In a study using confocal laser scanning microscopy with a fluorescent derivative of phalloidin, it was found that the mr cell contains actin filaments, but only in the apical pole and just below the outward-facing membrane [64]. The dynamic equilibrium between actin filaments and actin molecules is displaced by cytochalasins, which bind to one end of the filament. As a result, addition of actin molecules to that end is prevented, and in a short time, *F*-actin is depolymerised. The results presented in Fig. 12

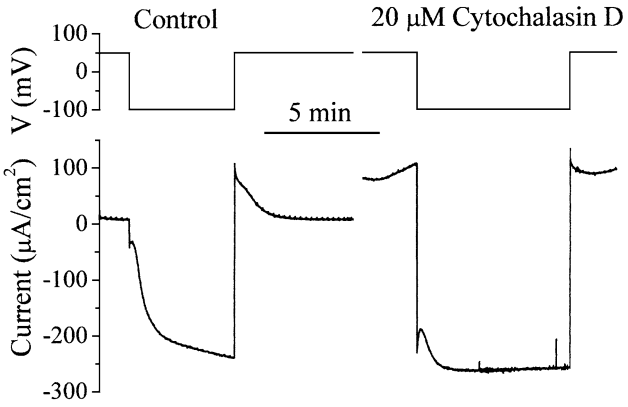

Fig. 12. Depolymerisation of *F*-actin by cytochalasin D eliminates deactivation of the voltage-controlled Cl^- conductance of mr cells. NaCl–Ringer's on the inside, KCl–Ringer's on the outside. To the left is shown the time course of the reversible Cl^- current activation obtained by stepping the transepithelial voltage from a holding value of +50 to −100 mV, and back. To the right is shown the current response to a similar voltage-clamp protocol after addition of 20 μM cytochalasin D to the solution bathing the inside of the isolated epithelium. At $V=-100$ mV, the Cl^- conductance is similar to that of the preparation in the control period, but the Cl^- conductance does no more deactivate following return of *V* to the holding value of +50 mV (unpublished).

indicate that addition of cytochalasin D prevents deactivation of the Cl^- conductance. In four experiments using this protocol, the maximally activated conductances ($V=-100$ mV) were 2430 ± 166 μS/cm^2 (control) and 2269 ± 160 μS/cm^2 (20 μM cytochalasin D), respectively. In a study on the regulation of membrane trafficking associated with proton secretion by oxyntic cells of the bullfrog gastric mucosa, it was indicated that cytochalasin besides inhibiting the secretory process also activates a paracellular conductance [65]. A similar effect on the paracellular pathway in this set of experiments on the toad skin epithelium is unlikely, as our study shows a small inhibition of the total conductance by cytochalasin, however, not statistically significant, $\Delta G=-161\pm126$ μS/cm^2 ($P=0.46$, paired two-tailed Student's *t*-test). Thus, it is indicated that the apically located actin molecules of the mr cells have to be assembled into filaments for the activated conductance to deactivate again. This working hypothesis is compatible with the notion forwarded above that processes in a submembrane domain participate in the control of the apical membrane's Cl^- conductance.

5. The voltage- and receptor-controlled Cl^- conductances are mutually exclusive

When the voltage-activated conductance of the mr cell is fully activated, application of cAMP does not lead to further activation of the chloride conductance [30]. As shown in Fig. 13A, stimulation by isoproterenol eliminated the voltage activation; however, the conductance at −100 mV was similar to the fully voltage-activated conductance before

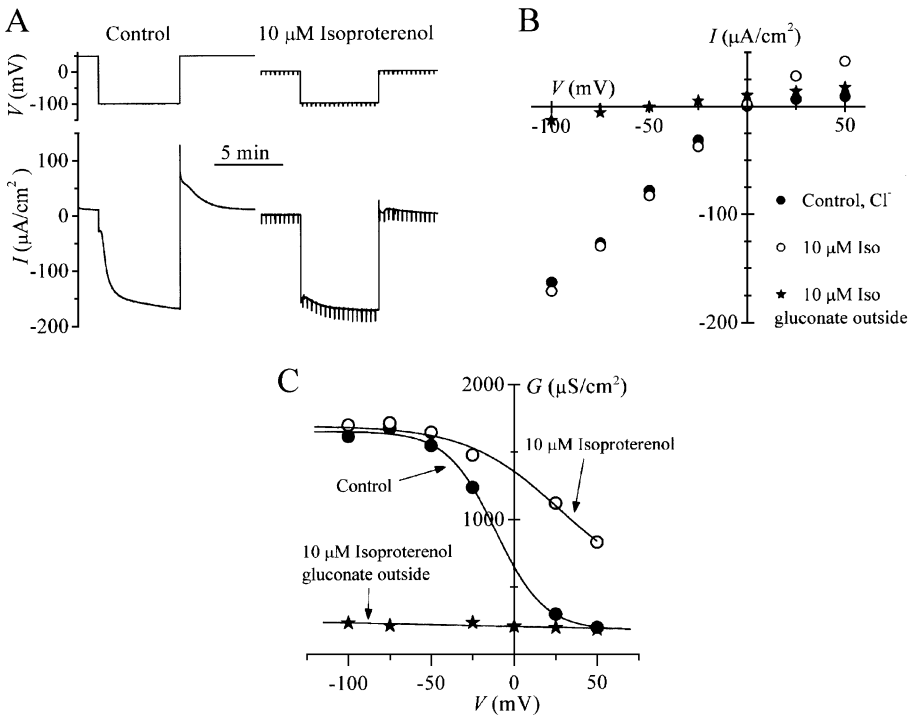

Fig. 13. (A) Time course of Cl^- current response of mr cells to stepping the transepithelial potential difference to −100 mV. NaCl–Ringer's on the inside, KCl–Ringer's on the outside. Following receptor activation by isoproterenol, the Cl^- conductance is already fully activated at −100 mV. (B) Current–voltage curves of the preparation during the control period, following receptor stimulation by isoproterenol, and in the absence of Cl^- in the outside solution ('10 μM isoproterenol, gluconate outside'). (C) Conductance–voltage relationships during the three periods. The conductance was calculated as, $G = I/(V - V_{rev})$. With gluconate, the reversal potential, $V_{rev} = -50$ mV, while $V_{rev} = \sim 0$ mV for the two other I–V relationships (unpublished).

activation via the β-adrenergic receptor (Fig. 13B,C). In the presence of isoproterenol, with gluconate on the outside, the reversal potential of the transepithelial current–voltage relationship was shifted to −50 mV (Fig. 13B). Qualitatively, this can be accounted for by the receptor-activated chloride permeability of the mr cells, which conducts chloride also in the outward direction. Isoproterenol did not significantly affect the 'leak' conductance of the preparation as is seen from the G–V relationship of the preparation bathed on the outside with a chloride-free solution ('gluconate outside', Fig. 13C). In our 1992 paper [30], it was stated that cAMP treatment displaced the G–V relationship to the right along the V-axis as is seen also from Fig. 13C. Based upon the effect of cAMP on the voltage-activated chloride conductance [52] and a pharmacological study of the cAMP and voltage-activated chloride conductances [66], Nagel et al. also suggested that it is the same Cl^- pathway that is being regulated in two different ways. Our more recent studies would suggest that the voltage- and the receptor-controlled Cl^- conductance are mediated via different populations of chloride channels in the apical membrane of the mr cell (cf. Figs. 8 and 10). Furthermore, as discussed above, the halide ion selectivity of the two pathways appears to be quite different with $P_{Br} > P_{Cl} > P_I$ for the voltage-activated pathway, and $G_{Cl} > G_B \gg G_I$ for the receptor-activated pathway. Although different methods were used for the selectivity studies, the findings mentioned would suggest that we are dealing with two different populations of chloride channels.

6. Biological significance and concluding remarks

The mr cell of amphibian skin epithelium is differentiated as a highly specialised pathway for chloride uptake. Two types of apical Cl^- pathways have been discussed above (see Fig. 14).

(i) The conductance of one of the pathways is controlled by voltage and external chloride concentration in such a way that the channels open only if $[Cl^-]_o$ is in the millimolar range and if the electrical potential is of a polarity that secures an inwardly directed net flux of this ion. Macroscopic studies lead to the conclusion that the external regulatory binding site is highly specific for Cl^-, whereas the anion selectivity of the conducting channel is poor. Reversible voltage activations of this conductance proceed with long time constants (10 s), which depend on the transepithelial potential difference, V, in such a way that the rate of conductance activation increases with increasing amplitude of V. Depolymerisation of apical F-actin by cytochalasin D removes the V-dependent deactivation of the conductance. The single-channel conductance has been estimated by noise analysis to be in the range of 150–300 pS. A channel of this size has been identified in the apical

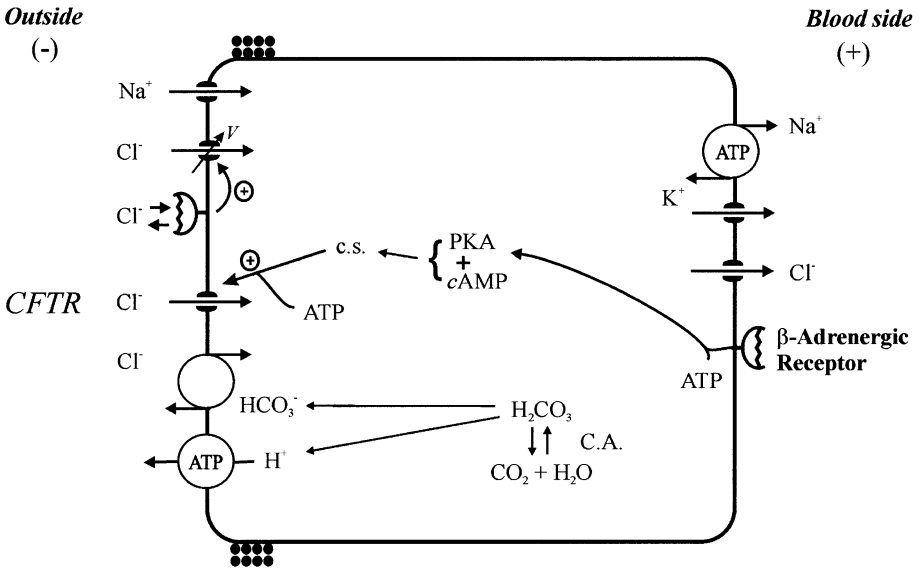

Fig. 14. Model of mr cell of *B. bufo* skin epithelium (modified from Ref. [71]). Included are the two pathways for passive uptake of Cl^-, which have been discussed in the present review. The activity of the cloned CFTR is supposed to be controlled by a basolateral β-adrenergic receptor via PKA, but in the text is discussed that also a PKC pathway may be involved. The other apical Cl^- channel has not been cloned. It is controlled by the apical membrane voltage via an unknown mechanism and by binding of Cl^- to an external site. At low external $[Cl^-]_o$, this channel is shut, and an active mechanism takes over the uptake of Cl^-, which is driven by a proton ATPase in parallel with a Cl^-/HCO_3^- exchanger. The active uptake of Cl^- was studied in Refs. [67–72]. The active uptake of Na^+ via an amiloride blockable apical sodium channel and a basolateral Na,K-ATPase was studied in Ref. [34]. c.s.: catalytic subunit of PKA; C.A.: carbonic anhydrase.

membrane of mr cells by patch clamping, but its biophysical properties have not been characterised at this level of resolution. The channel has not been cloned.

(ii) The other identified Cl^- pathway of mr cells is regulated via β-adrenergic receptors. The selectivity, pharmacology, and receptor activation indicate that this conductive pathway is due to CFTR chloride channels in the apical plasma membrane. *bb*CFTR of toad skin epithelium has been cloned, and immunostaining has shown that the gene product is selectively expressed in mr cells. Single-channel patch-clamp studies verified the expression of a small Cl^- channel with a limiting conductance (120 mM $[Cl^-]$/120 mM $[Cl^-]$) of 7 pS in this membrane, but its regulation at the molecular level has not yet been studied in sufficient detail.

There are interactions between the two passive pathways in the sense that activation of the conductance via receptor stimulation with isoproterenol excludes further conductance activation by voltage clamping, and vice versa. The mechanism of this interaction is unknown. The large conductance Cl^- channel, which by noise analysis was associated with the voltage-regulated pathway, exhibited substates in single-channel recordings often with openings and closures in steps. Thus, this large conductance channel may be composed of small channels of concerted activity. Small and large conductance channels have been resolved in the same patch, but it is unknown whether they are related to one another.

The skin is also capable of active uptake of Cl^- [67–72], which is of significance in freshwater of low [NaCl] concentration. Under this condition, and independent of the transepithelial potential difference, the voltage- and $[Cl^-]_o$-controlled chloride conductance is inactivated. Since there is a net uptake of Cl^- from freshwater [66] it would have to be assumed that the receptor-activated CFTR pathway is inactivated too. Our hypothesis of a H-ATPase-driven uptake of Cl^- (Fig. 14) is not in conflict with the hypothesis forwarded by Harvey [73], who assumed that the function of the apical H-ATPase is to hyperpolarize the apical membrane for driving Na^+ across the apical membrane. Both functions may be of significance.

Like the majority of other amphibians, the Bufonidae are dependent on freshwater during their brief breeding season, but otherwise, they are adapted to a terrestrial life with some species inhabiting estuarine waters with higher concentrations of salt (in which they also breed). The passive mechanisms for Cl^- uptake by the skin are supposedly the result of an adaptation to osmoregulation in water with [NaCl]>2–5 mM, where the thermodynamic work done in moving the two ions through the epithelium requires the activity of the Na,K-ATPase, only [28]. The function of the receptor-controlled CFTR chloride pathway is more difficult to comprehend. Toads that rehydrate from water pools or free water surfaces on land are capable of solute-coupled water uptake [74], and take up water even if the external osmotic concentration is the same as that of the body fluids [75–77]. One may speculate that the CFTR pathway is of significance under these conditions of solute-coupled water uptake.

Acknowledgements

Thanks are due to Ms. Hanne Schaltz and Mr. Thomas Sørensen for excellent technical assistance. The work was supported by grants from the Danish Natural Science Research Council, the Carlsberg Foundation, the Novo-Nordisk Foundation, and the Alfred Benson Foundation.

References

[1] H.H. Ussing, K. Zerahn, Active transport of sodium as the source of electric current in the short-circuited isolated frog skin, Acta Physiol. Scand. 23 (1951) 110–127.
[2] J.J. Grantham, M.B. Burg, J. Orloff, The nature of transtubular Na and K transport in isolated rabbit renal collecting tubules, J. Clin. Invest. 49 (1970) 434–441.
[3] B. Lindemann, W. Van Driessche, Sodium specific membrane channels in frog skin are pores: current fluctuations reveal high turnover, Science 195 (1977) 292–294.
[4] C.M. Canessa, L. Schild, G. Buell, B. Thorens, I. Gautschi, J.-D. Horisberger, B.C. Rossier, Amiloride sensitive epithelial sodium channel is made of three homologous subunits, Nature 367 (1994) 463–467.
[5] H. Garty, L.C. Palmer, Epithelial sodium channels: function, structure and regulation, Physiol. Rev. 77 (1997) 359–396.
[6] W. Nagel, W. Hirschmann, K^+-permeability of the outer border of the frog skin (*R. temporaria*), J. Membr. Biol. 52 (1980) 107–113.
[7] L.W. Frazier, J.C. Vanatta, Excretion of K^+ by frog with rate varying with K^+ load, Comp. Biochem. Physiol., A 90 (1981) 157–160.
[8] R. Nielsen, Active transepithelial potassium transport in frog skin via specific potassium channels in the apical membrane, Acta Physiol. Scand. 120 (1984) 287–296.
[9] W. Van Driessche, Physiological role of apical potassium channels in frog skin, J. Physiol. 356 (1984) 79–95.
[10] L. Palmer, Potassium secretion and the regulation of the distal nephron K channels, Am. J. Physiol. 277 (1999) F821–F825.
[11] L.C. Stoner, S.C. Viggiano, Environmental KCl causes an upregulation of apical membrane maxi K channels and ENaC channels in everted *Ambystoma* collecting tubules, J. Membr. Biol. 162 (1997) 107–116.
[12] N. Møbjerg, E.H. Larsen, I. Novak, K^+ transport in the mesonephric collecting duct system of the toad, *Bufo bufo*. Microelectrode recordings from isolated and perfused tubules, J. Exp. Biol. 205 (2002) 897–904.
[13] N.J. Willumsen, E.H. Larsen, Membrane potentials and intracellular Cl^- activity of toad skin epithelium in relation to activation and deactivation of the transepithelial Cl^- conductance, J. Membr. Biol. 94 (1986) 173–190.
[14] E. Schlatter, R. Greger, J.A. Schafer, Principal cells of cortical collecting ducts of rats are not route of transepithelial Cl^- transport, Pflügers Arch. 417 (1990) 317–323.
[15] W. Bargmann, U. Welsch, Über Kanälchenzellen und dunkle Zellen in Nephron von Anuren, Zetschr. Zellforsch. Mikroskop. Anat. 134 (1972) 193–204.
[16] N. Møbjerg, E.H. Larsen, Å. Jespersen, Morphology of the nephron in the mesonephros of *Bufo bufo* (Amphibia, Anura, Bufonidae), Acta Zool. 79 (1998) 31–50.
[17] W. Dantzler, Comparative aspects of renal function, In: D.W. Seldin, G. Giebisch (Eds.), The Kidney: Physiology and Pathophysiology, 2nd ed., Raven Press, New York, 1992, pp. 885–942.
[18] M. Whitear, Flask cells and epidermal dynamics in frog skin, J. Zool. Lond. 175 (1974) 107–149.
[19] J.K. Choi, The fine structure of the urinary bladder of the toad, *Bufo marinus*, J. Cell Biol. 16 (1963) 53–72.
[20] A.B. Keys, E.N. Willmer, Chloride secreting cells in the gills of fishes with special reference to the common eel, J. Physiol. 76 (1932) 368–378.
[21] D. Brown, J.L. Stow, Protein trafficking and polarity in kidney epithelium: from cell biology to physiology, Physiol. Rev. 76 (1996) 245–297.
[22] G. Giebisch, W. Wang, Potassium transport: from clearance to channels and pumps, Kidney Int. 49 (1996) 1624–1631.
[23] E.H. Larsen, Chloride transport by high-resistance epithelia, Physiol. Rev. 71 (1991) 235–283.
[24] P.E. Budtz, B.C. Christoffersen, J.S. Johansen, I. Spies, N.J. Willumsen, Tissue kinetics, ion transport, and recruitment of mitochondria-rich cells in the skin of the toad (*Bufo bufo*) in response to exposure to distilled water, Cell Tissue Res. 280 (1994) 65–75.
[25] U. Katz, S. Gabay, Dynamics and density of mitochondria-rich cells in toad skin epithelium, Biol. Cell 85 (1995) 185–190.
[26] E.H. Larsen, P. Kristensen, Properties of a conductive chloride pathway in toad skin, Acta Physiol. Scand. 102 (1978) 1–21.
[27] L.B. Kirschner, The study of NaCl in aquatic animals, Am. Zool. 10 (1970) 365–376.
[28] E.H. Larsen, L.J. Jensen, Å. Jespersen, N. Møbjerg, J.B. Sørensen, N.J. Willumsen, Chloride channels of mitochondria-rich cells in anuran skin: physiological significance and regulation, Zoology 99 (1995/96) 227–236.
[29] J. Ehrenfeld, Active proton and urea transport by amphibian skin, Comp. Biochem. Physiol. 119A (1998) 35–45.
[30] N.J. Willumsen, L. Vestergaard, E.H. Larsen, Cyclic-AMP and β-agonist activated chloride conductance of a toad skin epithelium, J. Physiol. 449 (1992) 641–653.
[31] P. Kristensen, Is chloride transfer in frog skin localized to a special cell type? Acta Physiol. Scand. 113 (1981) 123–124.
[32] C.L. Voûte, W. Meyer, The mitochondria-rich cells of frog skin as hormone sensitive 'shunt path', J. Membr. Biol. 40 (1978) 141–165.
[33] J.K. Foskett, H.H. Ussing, Localization of chloride conductance to mitochondria-rich cells in frog skin epithelium, J. Membr. Biol. 91 (1986) 251–258.
[34] E.H. Larsen, H.H. Ussing, K.R. Spring, Ion transport by mitochondria-rich cells in toad skin, J. Membr. Biol. 99 (1987) 25–40.
[35] E.H. Larsen, B.J. Harvey, Chloride currents of single mitochondria-rich cells of toad skin epithelium, J. Physiol. 478 (1994) 7–15.
[36] J.B. Sørensen, E.H. Larsen, Heterogeneity of chloride channels in the apical membrane if isolated mitochondria-rich cells from toad skin, J. Gen. Physiol. 108 (1996) 421–433.
[37] N.J. Willumsen, E.H. Larsen, Identification of anion-selective channels in the basolateral membrane of mitochondria-rich cells, J. Membr. Biol. 157 (1997) 255–269.
[38] W. Nagel, P. Somieski, A.M. Shipley, Mitochondria-rich cells and voltage activated chloride current in toad skin epithelium: analysis with scanning vibrating electrode technique, J. Membr. Biol. 161 (1998) 131–140.
[39] P. Somieski, W. Nagel, Localizing transepithelial conductive pathways using a vibrating voltage probe, J. Exp. Biol. 201 (1998) 2489–2495.
[40] K.-W. Yau, P.A. McNaughton, A.L. Hodgkin, Effect of ions on the light sensitive current in retinal rods, Nature 292 (1981) 502–505.
[41] E.H. Larsen, P. Kristensen, S. Nedergaard, N.J. Willumsen, Role of mitochondria-rich cells for passive chloride transport—with a discussion of Ussing's contributions to our understanding of shunt pathways in epithelia, J. Membr. Biol. 184 (2001) 247–254.
[42] W. Nagel, U. Katz, Trypsin inhibits voltage-activated chloride conductance of toad skin, Comp. Biochem. Physiol., Part A 122 (1999) 109–115.
[43] E.H. Larsen, P. Kristensen, Properties of a conductive cellular chloride pathway in the skin of the toad (*Bufo bufo*), Acta Scand. Physiol. 102 (1978) 1–21.
[44] E.H. Larsen, P. Kristensen, Effect of anoxia and of theophylline on transcellular Cl^- transport in toad skin, Proc. 27th Int. Congr. Physiol. Sci. Paris 13 (1977) 1002.

[45] W. Nagel, U. Katz, Cyanide inhibition of chloride conductance across toad skin, J. Membr. Biol. 173 (2000) 117–125.
[46] V. Koefoed-Johnsen, H.H. Ussing, The nature of the frog skin potential, Acta Physiol. Scand. 42 (1958) 298–308.
[47] P. Kristensen, Chloride transport in frog skin, In: J.A. Zadunaisky (Ed.), Transport Mechanisms in Epithelia, Academic Press, London, 1982, pp. 310–332.
[48] A.F. Harck, E.H. Larsen, Concentration dependence of halide fluxes and selectivity of the anion permeability in toad skin, Acta Physiol. Scand. 128 (1986) 289–304.
[49] F.J. Sigworth, Interpreting power spectra from nonstationary membrane current fluctuations, Biophys. J. 35 (1981) 289–300.
[50] I. De Wolf, W. Van Driessche, W. Nagel, Forskolin activates gated Cl^- channels in frog skin, Am. J. Physiol. 256 (1989) C1239–C1249.
[51] W. Nagel, W. Van Driessche, Chloride-related current fluctuations in amphibian skin, Pflügers Arch. 418 (1991) 544–550.
[52] U. Katz, W. Nagel, Effects of cyclic AMP and theophylline on chloride conductance across toad skin, J. Physiol. 489 (1995) 105–114.
[53] J. Amstrup, J. Frøslev, N.W. Willumsen, N. Møbjerg, Å. Jespersen, E.H. Larsen, Expression of cystic fibrosis transmembrane conductance regulator in the skin of the toad, *Bufo bufo*—possible role for Cl^- transport across the heterocellular epithelium, Comp. Biochem. Physiol., Part A 130 (2001) 539–550.
[54] A. Hipper, M. Mall, R. Greger, K. Kunzelmann, Mutations in the putative pore-forming domain of CFTR do not change anion selectivity of the cAMP activated Cl^- conductance, FEBS Lett. 374 (1995) 312–316.
[55] M.K. Mansoura, S.S. Smith, A.D. Choi, N.W. Richards, T.V. Strong, M.L. Drumm, F.S. Collins, D.C. Dawson, Cystic fibrosis transmembrane conductance regulator (CFTR) anion binding as a probe of the pore, Biophys. J. 74 (1998) 1320–1332.
[56] W. Nagel, U. Katz, α_1-Adrenoreceptors antagonize activated chloride conductance of amphibian skin epithelium, Pflügers Arch. - Eur. J. Physiol. 436 (1998) 863–870.
[57] T.-C. Hwang, G. Nagel, A.C. Nairn, D.C. Gadsby, Regulation of the gating of cystic fibrosis transmembrane conductance regulator Cl channels by phosphorylation and ATP hydrolysis, Proc. Natl. Acad. Sci. U. S. A. 91 (1994) 4698–4702.
[58] D.N. Sheppard, M.J. Welsh, Structure and function of the CFTR chloride channel, Physiol. Rev. 79 (1999) S23–S45.
[59] S.J. Tucker, D. Tannahill, C. Higgins, Identification and developmental expression of the *Xenopus laevis* cystic fibrosis transmembrane conductance regulator gene, Hum. Mol. Genet. 1 (1992) 77–82.
[60] J.R. Riordan, J.M. Rommens, B.-S. Kerem, N. Alon, R. Rozmehel, Z. Grzelczak, J. Zielenski, S. Lok, N. Plavsic, J.-L. Chou, M.L. Drumm, M.C. Iannuzzi, F.S. Collins, L.-C. Tsui, Identification of the cystic fibrosis gene: cloning and characterization of complementary DNA, Science 245 (1989) 1066–1073.
[61] B. Button, L. Reuss, G. Altenberg, PKC-mediated stimulation of amphibian CFTR depends on a single phosphorylation consensus site. Insertion of this site confers PKC sensitivity to human CFTR, J. Gen. Physiol. 117 (2001) 457–467.
[62] T.D. Singer, S.J. Tucker, W.S. Marshall, C.F. Higgins, A divergent CFTR homologue: highly regulated salt transport in the euryhaline teleost *F. heteroclitus*, Am. J. Physiol. 274 (1998) C715–C723.
[63] J.M. Chen, C. Cutler, C. Jacques, G. Bæuf, E. Denamur, G. Lecointre, B. Mercier, G. Cramb, C. Férec, A combined analysis of the cystic fibrosis transmembrane conductance regulator: implications for structure and disease models, Mol. Biol. Evol. 18 (2001) 1771–1781.
[64] N.J. Willumsen, J.W. Mills, Distribution of cytoskeletal proteins in toad skin epithelium, FASEB J. 12 (1998) A729.
[65] T.A.A.-G. Al-Shaibani, S.J. Hagen, Regulation of acid secretion and paracellular permeability by F-actin in the bullfrog, *Rana catesbeiana*, Am. J. Physiol. 282 (2002) G519–G526.
[66] W. Nagel, P. Somieski, U. Katz, Selective inhibition of Cl^- conductance in toad skin by blockers of Cl^- channels and transporters, Am. J. Physiol. 281 (2001) C1223–C1232.
[67] A. Krogh, Osmotic regulation in the frog (*R. esculenta*) by active absorption of chloride ions, Skand. Arch. Physiol. 76 (1937) 60–74.
[68] J.A. Zadunaisky, O.A. Candia, D.J. Chiarandini, The origin of the short-circuit current in the isolated skin of the South American frog *Leptodactyllus ocellatus*, J. Gen. Physiol. 47 (1963) 393–402.
[69] P. Kristensen, Chloride transport across isolated frog skin, Acta Physiol. Scand. 84 (1972) 338–346.
[70] J. Ehrenfeld, F. García-Romeu, Coupling between chloride absorption and base excretion in isolated skin of *Rana esculenta*, Am. J. Physiol. 235 (1978) F33–F39.
[71] L.J. Jensen, J.N. Sørensen, E.H. Larsen, N.J. Willumsen, Proton pump activity of mitochondria-rich cells. The interpretation of external proton-concentration gradients, J. Gen. Physiol. 109 (1997) 73–91.
[72] L.J. Jensen, N.J. Willumsen, E.H. Larsen, Proton pump activity is required for active uptake of chloride in isolated amphibian skin exposed to freshwater, J. Comp. Physiol. B 172 (2002) 503–511.
[73] B.J. Harvey, Energization of sodium absorption by the H^+-ATPase pump in mitochondria-rich cells of frog skin, J. Exp. Biol. 172 (1992) 289–309.
[74] P.A. Sullivan, K. von Seckendorff Hoff, S.D. Hillyard, Effects of anion substitution on hydration behaviour and water uptake of the red-spotted toad, *Bufo punctatus*: is there an anion paradox in amphibian skin? Chem. Senses 25 (2000) 167–172.
[75] A. Durig, Wassergehalt und Organfunktion, Pflügers Arch. 85 (1901) 401–504.
[76] C.B. Jørgensen, 200 years of amphibian water economy: from Robert Townson to the present, Biol. Rev. 72 (1997) 153–237.
[77] S.D. Hillyard, E.H. Larsen, Lymph osmolality and rehydration from NaCl solutions by toads, *Bufo marinus*, J. Comp. Physiol., B 171 (2001) 283–292.